Available online at www.sciencedirect.com

ScienceDirect

journal homepage: http://www.elsevier.com/locate/rpor

Original research article

A depth dose study between AAA and AXB algorithm against Monte Carlo simulation using AIP CT of a 4D dataset from a moving phantom

Roger Cai Xiang Soh[a,b,*], *Guan Heng Tay*[c], *Wen Siang Lew*[b], *James Cheow Lei Lee*[b,c]

[a] *Department of Radiation Oncology, National University Cancer Institute, Singapore*
[b] *Division of Physics and Applied Physics, Nanyang Technological University, Singapore*
[c] *Division of Radiation Oncology, National Cancer Centre, Singapore*

ARTICLE INFO

Article history:
Received 20 September 2017
Received in revised form
15 May 2018
Accepted 9 August 2018
Available online 3 September 2018

Keywords:
Dose calculation algorithm
AXB
AAA
Monte Carlo

ABSTRACT

Aim: To identifying depth dose differences between the two versions of the algorithms using AIP CT of a 4D dataset.

Background: Motion due to respiration may challenge dose prediction of dose calculation algorithms during treatment planning.

Materials and methods: The two versions of depth dose calculation algorithms, namely, Anisotropic Analytical Algorithm (AAA) version 10.0 (AAAv10.0), AAA version 13.6 (AAAv13.6) and Acuros XB dose calculation (AXB) algorithm version 10.0 (AXBv10.0), AXB version 13.6 (AXBv13.6), were compared against a full MC simulated 6X photon beam using QUASAR respiratory motion phantom with a moving chest wall. To simulate the moving chest wall, a 4 cm thick wax mould was attached to the lung insert of the phantom. Depth doses along the central axis were compared in the anterior and lateral beam direction for field sizes $2 \times 2\,cm^2$, $4 \times 4\,cm^2$ and $10 \times 10\,cm^2$.

Results: For the lateral beam direction, the moving chest wall highlighted differences of up to 105% for AAAv10.0 and 40% for AXBv10.0 from MC calculations in the surface and buildup doses. AAAv13.6 and AXBv13.6 agrees with MC predictions to within 10% at similar depth. For anterior beam doses, dose differences predicted for both versions of AAA and AXB algorithm were within 7% and results were consistent with static heterogeneous studies.

Conclusions: The presence of the moving chest wall was capable of identifying depth dose differences between the two versions of the algorithms. These differences could not be identified in the static chest wall as shown in the anterior beam depth dose calculations.

* *Corresponding author at*: Department of Radiation Oncology, National University Cancer Institute, Singapore.
E-mail address: rsoh002@e.ntu.edu.sg (R.C.X. Soh).
URL: http://www3.ntu.edu.sg/home/wensiang/index.html (W.S. Lew).

https://doi.org/10.1016/j.rpor.2018.08.003
1507-1367/

1. Background

The calculation of photon field dose distributions within low-density inhomogeneity in the presence of motion artefacts can be a challenge for algorithms in clinical treatment planning systems (TPS). Such clinical cases with low-density inhomogeneity and motion artefacts are common for lung stereotactic body radiation therapy (SBRT) treatments. During lung SBRT planning, dose calculations are performed on average intensity projected (AIP) images derived from four-dimensional computed tomography (4DCT) images.[1] This accounts for any tumour motion due to respiration during treatment. As high doses are being delivered in few fractions during lung SBRT, dosimetric precision for dose calculations are relevant and very important.

Most inhomogeneity studies compare calculated depth doses within static inhomogeneous phantoms.[2–10] Other respiratory motion studies done were only limited to the superior–inferior tumour motion.[11,12] A controlled depth dose study of external surface motion and anterior–posterior tumour motion will contribute to the understanding of calculated dose distributions under respiratory motion. Furthermore, small photon fields such as $2 \times 2\,cm^2$ can impose problems due to lack of lateral charge particle equilibrium and changes in energy spectrum. Under the presence of motion artefacts, small photon fields and low-density medium such as lung, the limitations of clinical dose calculation algorithms can be tested.

Previous inhomogeneous phantom studies compared the performance of Anisotropic Analytical Algorithm (AAA) and Acuros XB dose calculation (AXB) algorithm (both from Varian Medical Systems, Inc., Palo Alto, CA), version 10.0.28, against Monte Carlo (MC) simulation. It was found that the accuracy of the algorithms depends on the photon beam energy, field size and density of the medium.[2–8] The recent release of an improved version for both AAA and AXB algorithms, version 13.6.23, highlighted key changes in the dose prediction performance, especially in how each algorithm account for inhomogeneities.

2. Aim

To our knowledge thus far, no was study done for the depth dose differences between a full MC simulation and two versions of AAA and AXB algorithm under the presence of a moving tumour and chest wall.

This study will systematically investigate the comparison of MC calculated depth doses from an independently modelled treatment head against independently simulated 6X depth doses calculated using AAA and AXB algorithm, versions 10.0.28 and 13.6.23. Dose calculations were done on the QUASAR respiratory motion phantom (Modus Medical Devices Inc., London, ON). Electron Gamma Shower Monte Carlo simulation package developed by the National Research Council of Canada (EGSnrc)[13] was used for the full Monte Carlo simulation. MC simulated data were validated against measurement under homogenous condition in water, as well as inhomogeneous condition in a static lung phantom. MC was used as a benchmark for depth dose comparison in the respiratory phantom for this study. Anterior and lateral beam depth doses were compared to investigate depth dose differences for both superior–inferior and anterior–posterior motion of the tumour.

3. Materials and methods

3.1. *Full Monte Carlo simulation model*

Monte Carlo calculations were done using EGSnrc V4-r2.4.0, consisting of BEAMnrc and DOSXYZnrc user codes developed by the National Research Council of Canada. A Linux-based computer cluster which comprised of 12 Intel Xeon central processing units (CPUs) with processing speeds of 2.67 or 3.4 GHz and a total of 40 GB of RAM was used for the calculations.

Phase space files for a Varian Clinac iX linear accelerator treatment head (Varian Medical Systems Inc., Palo Alto, CA) of 6 MV photon beam for field sizes $2 \times 2\,cm^2$, $4 \times 4\,cm^2$ and $10 \times 10\,cm^2$ (100 cm SSD) were generated using BEAMnrc. The initial electron beam was 6.1 MeV with focal spot width of 0.3 cm at full width at half maximum. The energy spectrum of the bremsstrahlung beam was matched with the phase space file released by International Atomic Energy Agency (IAEA) phase space database.[14] Computational efficiency was increased using variance reduction technique such as directional bremsstrahlung splitting (DBS). The global photon and electron cut-off energies were 0.01 MeV and 0.7 MeV respectively. The splitting number was set to 1000 and the electron splitting was performed in the lower layers of the flattening filter as recommended.[15] Range rejection was turned on with varying ECUTRR and was considered for electrons with energy less than 2 MeV (ESAVE_GLOBAL = 2).[16] EXACT was chosen for the boundary crossing and electron step algorithms. Both BEAMnrc and DOSXYZnrc usercodes used similar settings. All DOSXYZnrc dose calculations were performed using 1×10^{10} histories with statistical uncertainties below 1%. EGSnrc calculation voxel size was set similar to Eclipse treatment planning system (TPS) (Varian Medical Systems, Palo Alto, CA) calculation grid size of 0.25 cm. The uniform calculation grid size across considered algorithms was an improvement from the previous inhomogeneity dose modelling done by Zvolanek et al.[17]

3.2. *AAA and AXB algorithm*

AAA and AXB algorithm were configured for Varian Clinac iX using Eclipse TPS. Calculations were done across AAA version 10.0.28 (AAAv10.0), AAA version 13.6.23 (AAAv13.6), AXB algorithm version 10.0.28 (AXBv10.0) and AXB algorithm version 13.6.23 (AXBv13.6) against MC simulation. Dose to medium (D_m) reporting mode was chosen for AXBv10.0 and AXBv13.6, similar to previous studies.[6,7,18–20] From here on forth, the terms "AAA" and "AXB algorithm" will be used to describe both versions of their algorithms (i.e. AAAv10.0, AAAv13.6 and AXBv10.0, AXBv13.6 respectively). Depth dose profiles for field sizes $2 \times 2\,cm^2$, $4 \times 4\,cm^2$ and $10 \times 10\,cm^2$ were calculated with calculation grid size of 0.25 cm.

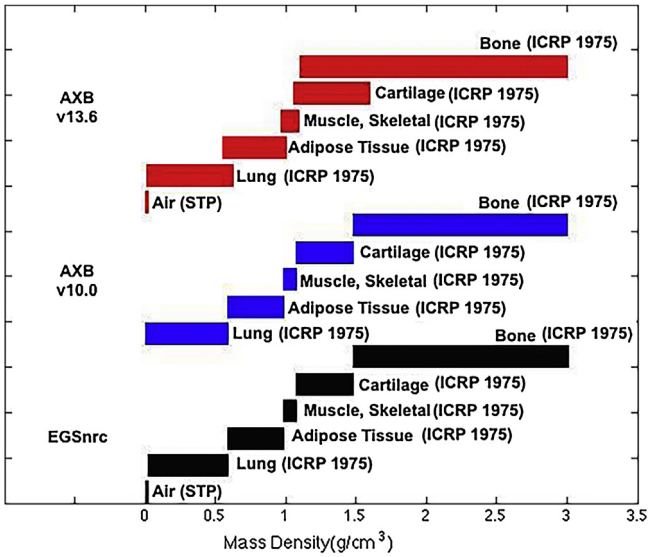

Fig. 1 – Material assignment for EGSnrc MC simulations, AXBv10.0 and AXBv13.6.

3.3. *CT calibration curve*

The CT calibration curve in Eclipse TPS was calibrated using a multi-plug CIRS® phantom 062 (Computerized Imaging Reference Systems, Norfolk, VA, USA). Both AXBv10.0 and AXBv13.6 refers to the same CT calibration curve for the HU value to mass density relationship in each voxel of the image grid. For consistency, the same CT calibration curve was configured in MC calculations. Cross section data for air, lung, adipose, muscle, cartilage and bone were generated according to AXBv10.0 material cross section data using PEGS in EGSnrc.[13,21] The HU value to relative electron density calibration curve for AAA calculations was also calibrated using the same phantom.

3.3.1. *Mass density to material mapping*

In order to perform dose calculations, AXB algorithm and EGSnrc require the macroscopic cross section for each material in its computational grid.[19] The algorithms, however, assign the material based on the HU value of each voxel differently. AXBv13.6 allows the overlapping of mass density ranges in CT to material mapping[22] (Fig. 1). In contrast, EGSnrc and AXBv10.0 do not allow the overlapping of mass density ranges. The mass density to material mapping for EGSnrc was configured to be the same as AXBv10.0, except with the addition of air material in EGSnrc. The air material added was identical to AXBv13.6. This was similar to previous work done by Ojala et al. and Onizuka et al.[23,24]

3.4. *Variations in HU profile under static and respiratory motion*

The moving lung tumour and chest wall causes motion artefacts, forming HU value gradients. This causes several regions of the lung phantom to exhibit contrasting HU values relative to the denser tumour polyoxymethylene sphere,[25] as shown in Fig. 2a and b. The AIP HU profile in the anterior beam direction shows less CT contrast and greater similarities to static HU

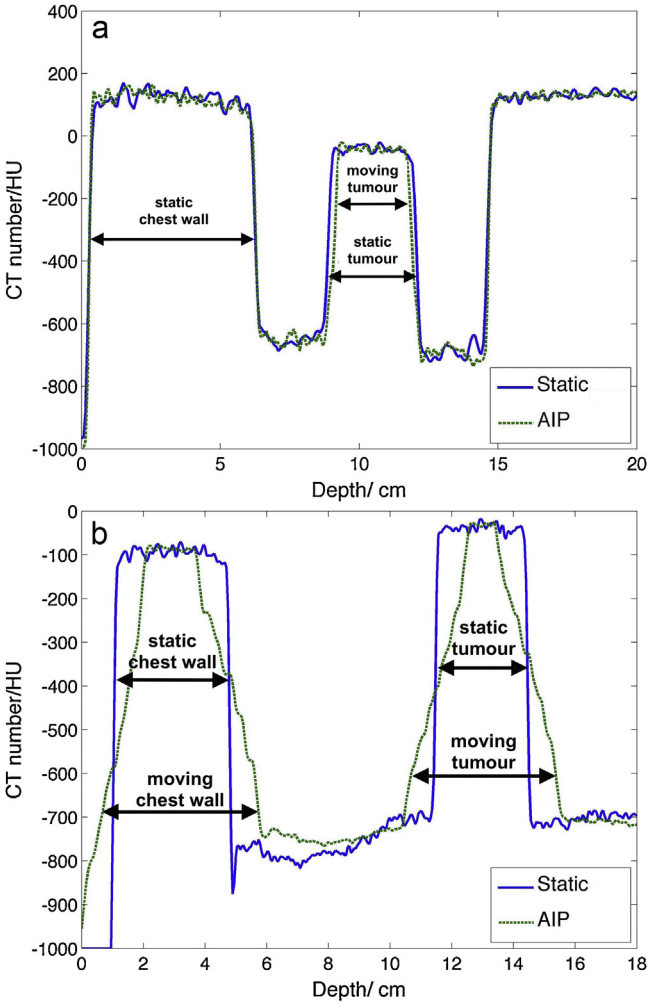

Fig. 2 – A comparison of the static tumour CT image (solid line) with the AIP CT image (dotted line).

profile. HU profile differences could only be observed for the superior–inferior tumour motion, with only a minor difference between HU value gradients.

In the lateral beam direction, the moving chest wall had a HU value gradient between −900 and −100 HU, representing the highest CT contrast due to motion.The moving chest wall and tumour dimensions were enlarged by twice the motion amplitude in the lateral beam AIP HU profile, with ill-defined boundaries between different mediums.

3.4.1. *Validation of MC doses under homogeneity condition*

MC depth dose profiles for field sizes $2 \times 2\,cm^2$, $4 \times 4\,cm^2$ and $10 \times 10\,cm^2$ were verified against an IBA PFD Photon Diode Dosimetry detector (IBA/Scanditronix Medical AB, Uppsala, Sweden) in water. The experimental setup comprises of a $30 \times 30 \times 30\,cm^3$ water phantom placed on the patient couch with the linear accelerator gantry at 270°. Correspondingly, water phantom was simulated using H2O700ICRU with a voxel size of $0.25 \times 0.25 \times 0.25\,cm^3$ in DOSXYZnrc. MC simulated data agreed with measured data and passed gamma analysis

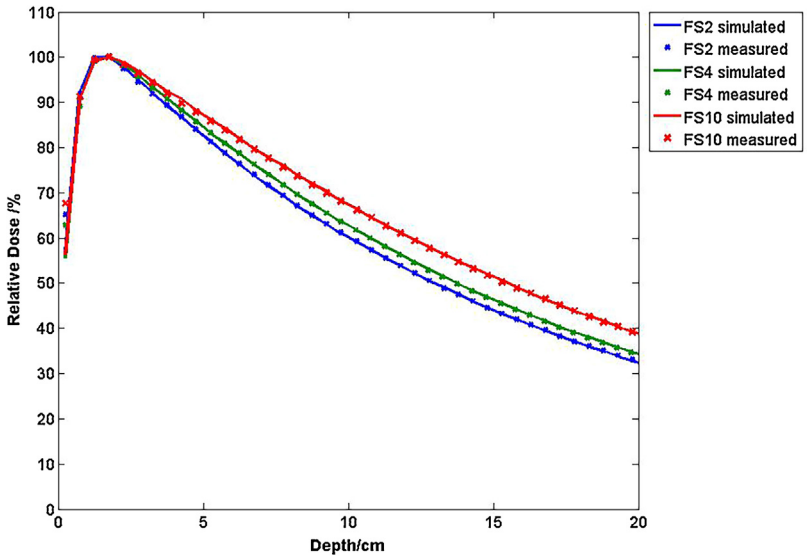

Fig. 3 – Verification of MC simulated PDD in water for field sizes 2 × 2 cm^2, 4 × 4 cm^2 and 10 × 10 cm^2.

with passing criteria of 1%/1 mm for the required field sizes in this study[26] (Fig. 3).

3.4.2. *Validation of MC calculated doses under inhomogeneous condition*

MC depth dose profiles for field sizes 2 × 2 cm^2, 4 × 4 cm^2 and 10 × 10 cm^2 were validated under inhomogeneous condition against film dosimetry. In-vivo measurements were done using Gafchromic™ External Beam Therapy 3(EBT3) films (International Specialty Products, Wayne, New Jersey). Absolute dosimetry was obtained by calibration of the required films to a known dose distribution during each measurement session. For each measurement position, the average data from two pieces of films was evaluated to increase the accuracy of the measured plane.[11,27] Films were scanned at 75 dots per inch (dpi) using Epson Expression 11000XL scanner (Seiko Epson Corporation, Nagano, Japan) at 15 h after the irradiation. Evaluation of film measurements was done using SNC Patient software (version 6.2.1, Sun Nuclear Corp., Melbourne, FL, USA).

Fig. 4a shows the experimental setup of the static lung phantom used. It consists of composite cork slabs sandwiched between 4 cm thick CIRS plastic water (Computerized Imaging Reference Systems Plastic Water Diagnostic Therapy, Norfolk, VA, USA) above and below. 14 pieces of 1 cm thick, composite cork slabs, with density 0.27 g/cm^3 were used. 14 film measurement positions were done along the central axis at 1.5 cm, 2 cm, 3 cm, 4 cm, 6 cm, 8 cm, 11 cm, 14 cm, 16 cm, 18 cm, 18.5 cm, 19 cm, 20 cm and 21 cm below the surface. Films were placed along the central axis at each position per measurement, so as to prevent overshadowing. The lung phantom was simulated in MC according to the weight fractions of the elements within the materials, as reported by Ramaseshan et al.[28] and Chang et al.[29] Calculation voxel size was 0.25 × 0.25 × 0.25 cm^3. Results show that MC simulated data agreed with film measured data to within 2% tolerance for the field sizes investigated (Fig. 4b).

3.5. *QUASAR respiratory motion phantom setup*

QUASAR respiratory motion phantom was configured to 1 cm amplitude sinusoidal respiratory motion, with a breathing frequency of 0.25 Hz. This corresponds to an average patient breathing amplitude and rate of 15 breaths/min.[30] The cedar wood lung insert holds a 3 cm diameter polyoxymethylene sphere which simulates the target lung tumour (Fig. 5).

Dental modelling wax was moulded to the lung phantom insert to create a 4 cm chest wall. The dental modelling wax used (Metrowax, Metrodent Limited, United Kingdom) is a tissue equivalent material that allows the simulation of the buildup dose before the cedar wood lung phantom insert.[31] Table 1 shows the density and material composition of the QUASAR lung insert materials.

3.6. *Image acquisition*

4DCT images were acquired using a single-source multidetector CT scanner (Siemens Somatom Definition AS, Siemens Medical Solutions, Forchheim, Germany). The 4DCT images using 1 mm slice thickness, 0.5 s per rotation and 0.1 pitch was obtained to construct the AIP images of the phantom. AIP images were obtained by averaging the ten phases of gated 4DCT images based on the helical Computed Tomography (CT) images.[35] These phases were obtained from the respiratory signal using the real-time position management optical system of the 4DCT (RPM; Varian Medical Systems, Palo Alto, CA).

3.7. *Beam delivery and normalisation*

6 MV photon beam was planned orthogonally at 100 cm fixed source to surface distance (SSD) setup when the lung insert is in the equilibrium position. The anterior beam was delivered orthogonal to the superior–inferior motion. The lateral beam was delivered in the direction of anterior–posterior motion with the moving chest wall, as shown in Fig. 6.

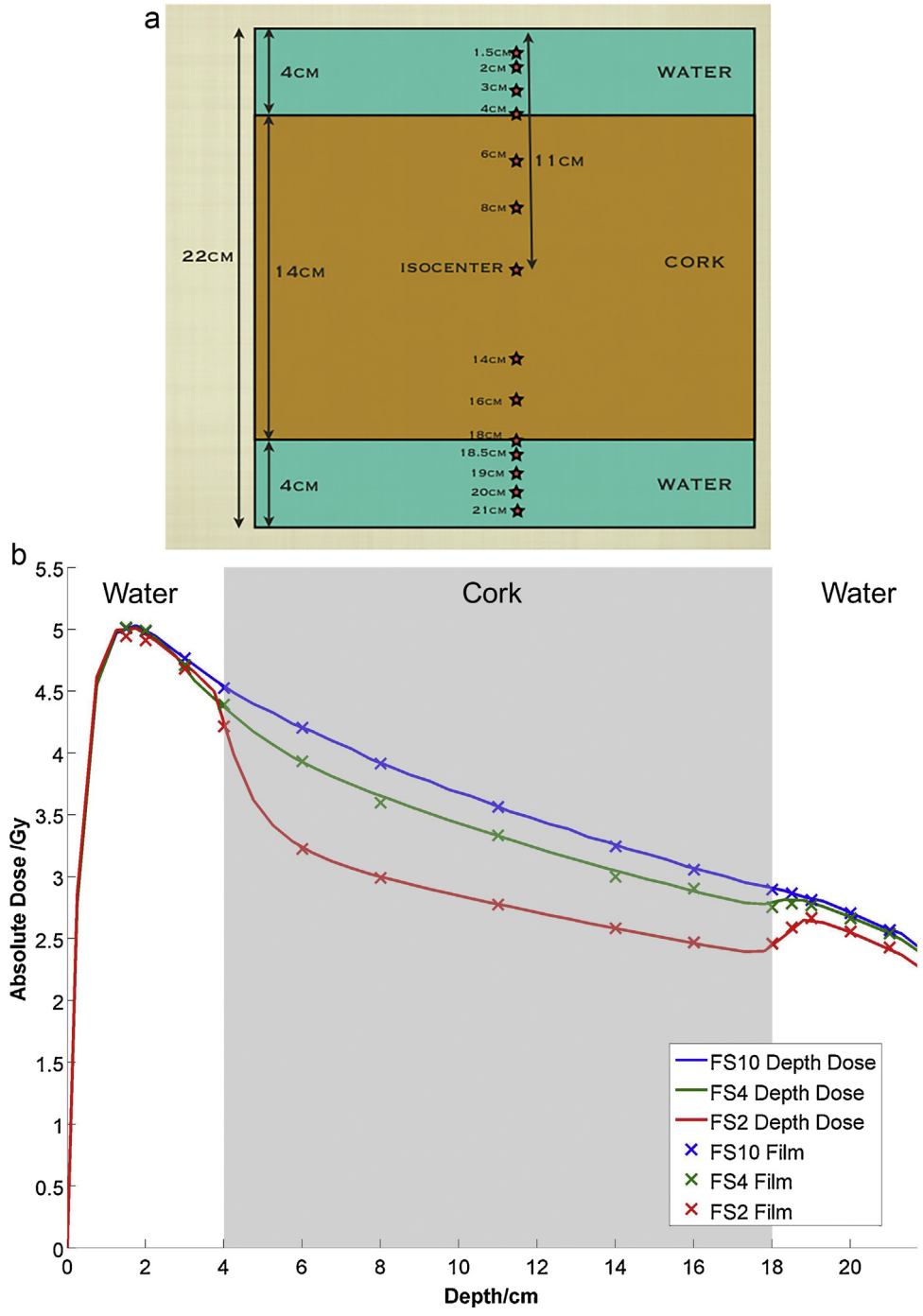

Fig. 4 – Verification of MC simulated depth dose in inhomogeneous lung phantom using film dosimetry at various measurement depth for field sizes 2 × 2 cm², 4 × 4 cm² and 10 × 10 cm².

For anterior beams, central axis depth dose profiles were normalised to the dose at 3 cm depth within the static chest wall (Fig. 7). For lateral beams, central axis depth dose profiles were normalised to the dose at 3 cm depth in the middle of the moving chest wall (Fig. 7). Normalisation was done within the chest wall instead of at the centre of the tumour because of statistical fluctuation of calculated dose to tumour from the full MC dose profile.

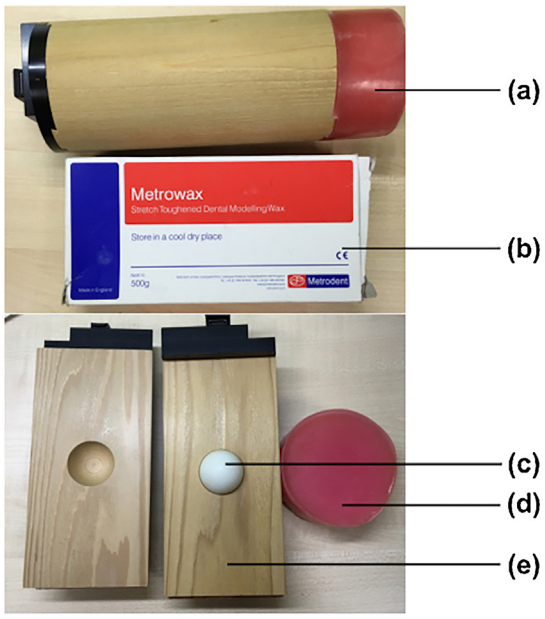

(a) Chest wall mould
(b) Metrowax
(c) Polyoxymethylene sphere
(d) Disassembled chest wall mould
(e) Disassembled cedar wood lung insert

Fig. 5 – The QUASAR lung insert.

Table 1 – QUASAR lung insert materials.

	Density (g/cm^3)	Material composition
Metrowax	0.85	Paraffin and microcrystalline waxes[32]
Polyoxymethylene sphere	1.41	$(CH_2O)_n$[33]
Cedar wood	0.26	6% H, 43% O, 50% C[34]

4. Results

4.1. *Depth dose comparison in the anterior beam direction*

Anterior depth doses are shown in Fig. 8. By comparing with MC results, AAA tends to predict lower doses after static chest wall–lung interface for $2 \times 2\,cm^2$ and $4 \times 4\,cm^2$ and higher

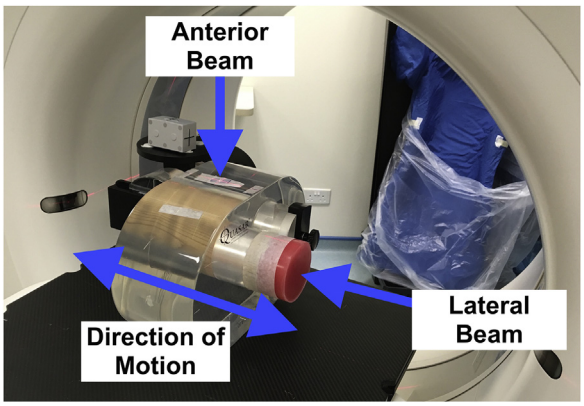

Fig. 6 – Experimental configuration on a QUASAR phantom.

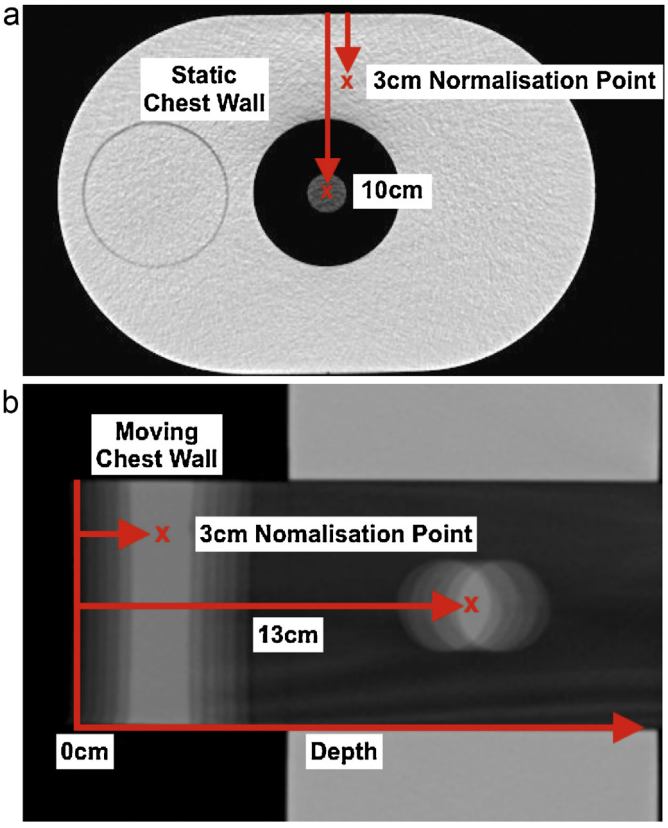

Fig. 7 – Normalisation point was defined at 3 cm depth within the static chest wall for the anterior beam and in the middle of moving chest wall at 3 cm depth for the lateral beam.

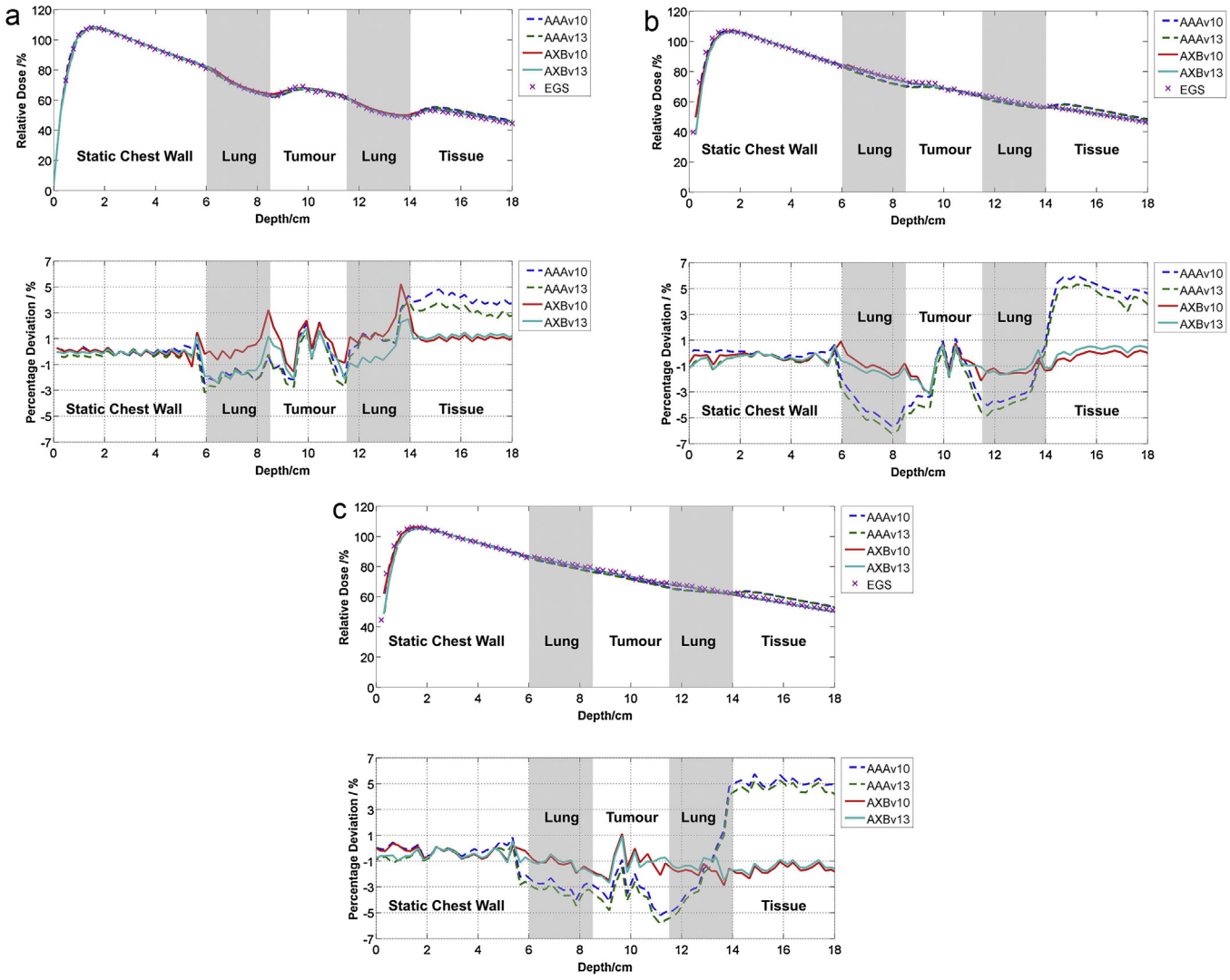

Fig. 8 – Depth dose profile of phantom in the anterior beam direction for field sizes 2 × 2 cm^2, 4 × 4 cm^2 and 10 × 10 cm^2. The subplot below the depth dose profile represents the percentage deviation of AAA and AXB algorithm predicted doses from MC simulation.

doses for all field sizes after lung–tissue interface. The greatest difference occurred for 10 × 10 cm^2 field, where deviations up to 7% was observed.

Predictions from AXB algorithm are generally within ±6% against MC simulation for all field sizes. The highest dose difference from MC was about 5.2% at lung–tissue interface in 2 × 2 cm^2 field by AXBv10. Deviations of AAA and AXB algorithm from MC calculations were within 7% even for the surface and buildup doses in the static chest wall. Results were consistent with previous static heterogeneous studies found.[2,5,6]

4.2. *Depth dose comparison in the lateral beam direction*

Fig. 9 shows the comparison of AAA and AXB algorithm predicted depth doses against MC simulation in the lateral beam direction. The largest deviation of up to 105% from MC simulation occurs at the surface and buildup doses in 2 × 2 cm^2 for AAAv10.0. For 10 × 10 cm^2, AXBv10.0 had 40% deviation in the surface and buildup doses from MC simulation. This disagreement of surface doses occurs at the high HU value gradient region in the moving chest wall. AAAv13.6 and AXBv13.6, on the contrary, shows agreement within 10% to MC simulation for all field sizes.

Excluding the surface and buildup regions, predictions by AAA algorithms show deviations in the secondary buildup regions such as the lung–tumour interfaces. This is especially so for field size 2 × 2 cm^2 (Fig. 9a). Predictions by AXB algorithm within the phantom was in good agreement with MC simulations for all field sizes (within ±4%) even in the presence of the anterior–posterior tumour motion.

4.3. *Differences between the two versions of AAA and AXB algorithm*

Generally, differences for AAA and AXB algorithm predicted depth doses, excluding the surface and buildup doses, agrees well with each other to within ±1.5% (Fig. 10).

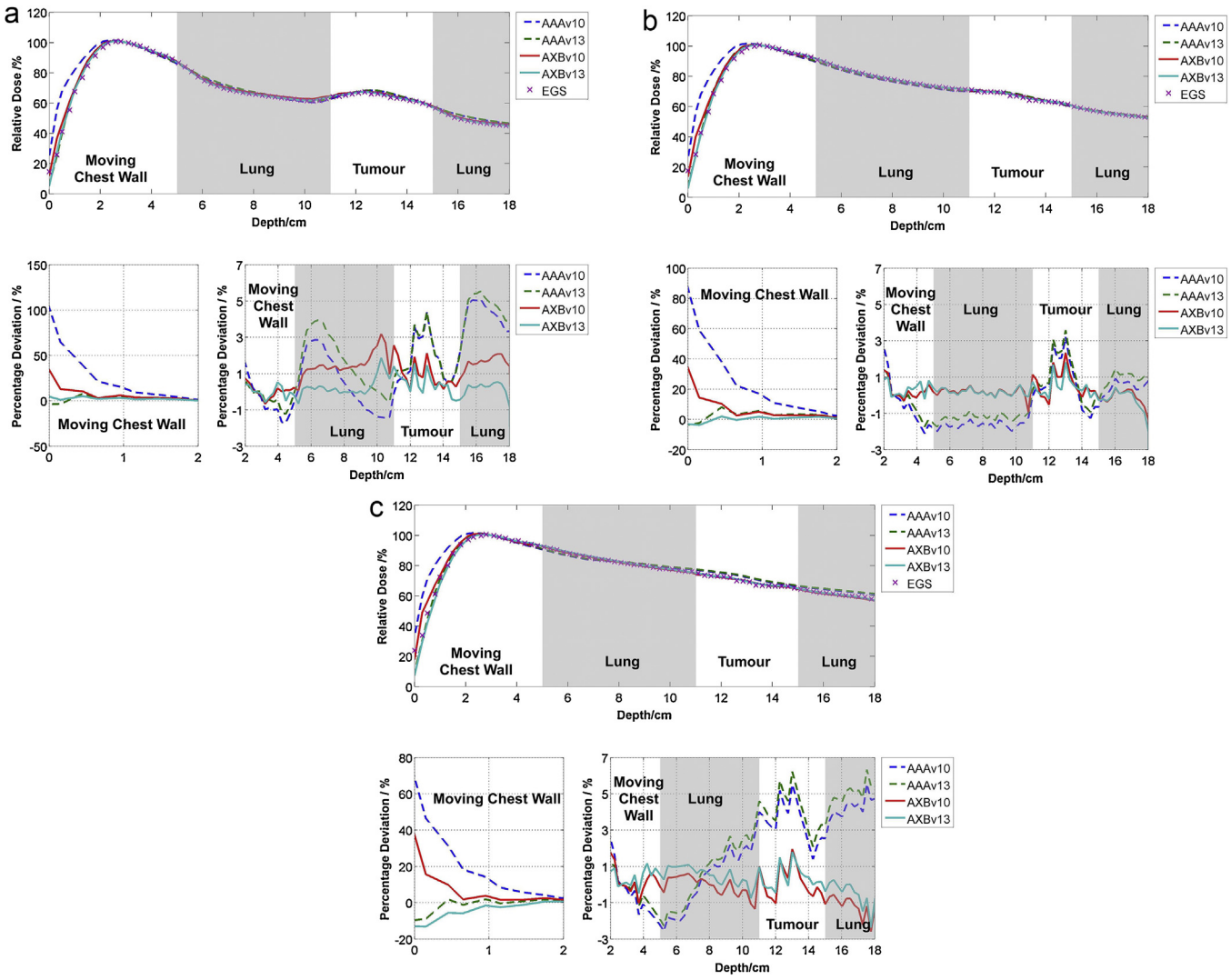

Fig. 9 – Depth dose profiles of moving tumour for field sizes 2 × 2 cm^2, 4 × 4 cm^2 and 10 × 10 cm^2. Beam was delivered in the lateral direction. The subplot below the depth dose profile shows the percentage deviation of AAA and AXB algorithm predicted doses from MC simulation. A separate plot shows the same result for the buildup region from 0 to 2 cm depth.

The surface and buildup doses for AAAv10.0 differs by up to 300% from AAAv13.6. Deviations in the surface and buildup doses between AXBv10.0 and AXBv13.6 differs by up to 60%.

5. Discussions

The depth dose comparison of a full MC simulation against dose calculations using AAA and AXB algorithm, versions 10.0.28 and 13.6.23 was investigated. The full MC simulation was verified under homogeneous and inhomogeneous conditions and was taken as the benchmark for this study.

Our results have highlighted large dose differences of up to 105% for AAAv10.0 and AXBv10.0 against the MC benchmark in the lateral beam direction. These differences were found in the region of the moving chest wall. Smaller dose differences were reported for AAAv13.6 and AXBv13.6. As discussed previously, the AIP CT of the moving chest wall has the highest HU value gradient due to the anterior–posterior motion. Previous studies claimed that anterior–posterior tumour motion was not clinically important because superior–inferior tumour motion was greater.[11,36] However, this study shows that by having an experimental setup for anterior–posterior tumour motion, together with a 4 cm moving chest wall and 1 cm amplitude, it creates a controlled, yet challenging and demanding inhomogeneity condition. Results show that this setup was capable of differentiating the dosimetric capabilities of each algorithm and its respective versions. Anterior beam direction for superior–inferior tumour motion results was in fact, consistent with previous static inhomogeneous phantom and inhomogeneity dose modelling with respiratory motion studies[2,5,6,11,12,17] but it was unable to differentiate the dosimetric capabilities of different algorithm versions. Dose differences in the surface and buildup regions in the

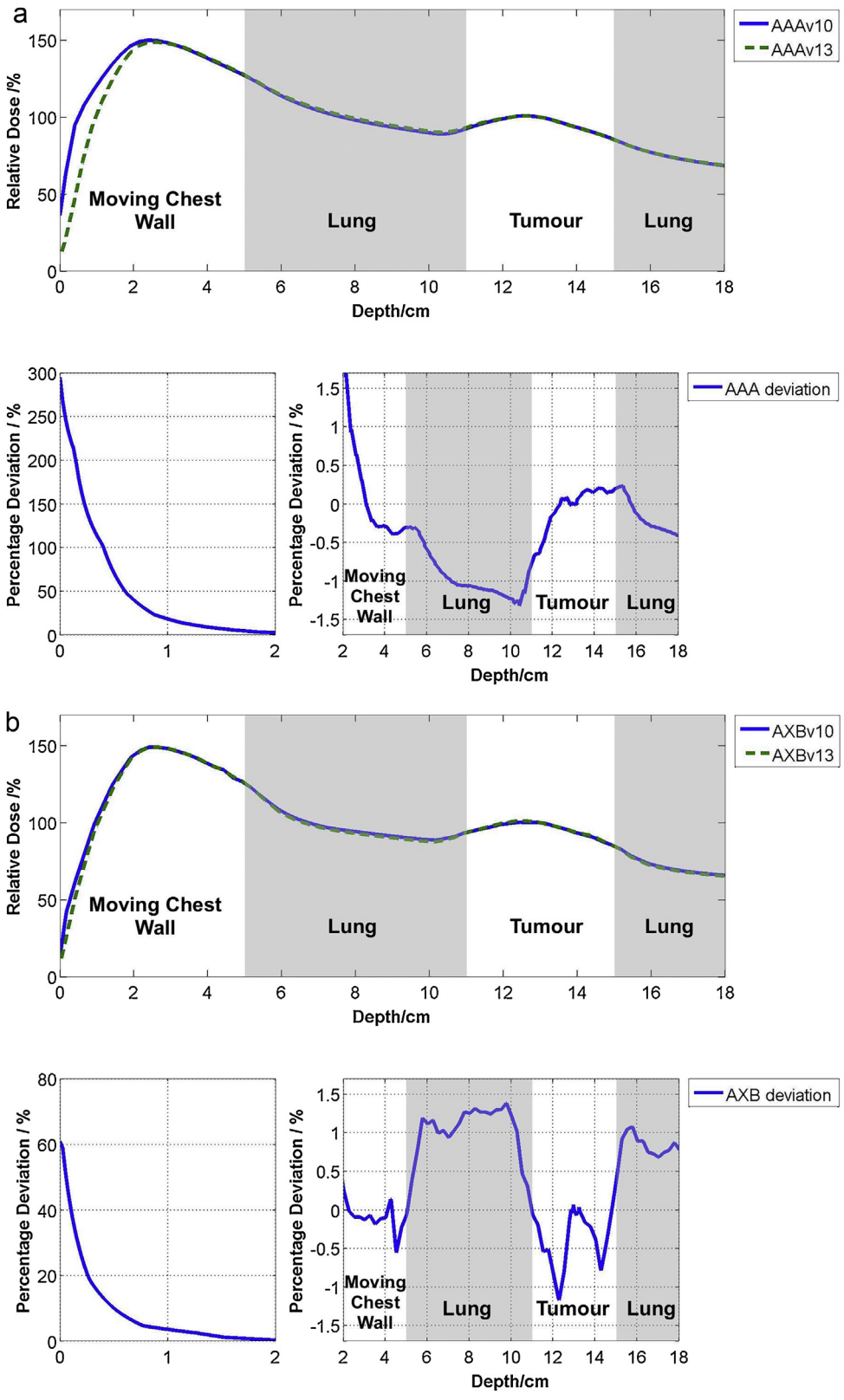

Fig. 10 – Comparison of the depth dose profiles of the two versions of the algorithms for field size 2 × 2 cm^2. Beam was delivered in the lateral direction. The subplot below the depth dose profile shows the percentage deviation between v10.0 with respect to depth doses predicted in v13.6. A separate plot shows their differences for 0–2 cm depth.

moving chest wall were not identified in the static chest wall as shown in the anterior beam depth dose calculations.

The revelation of the dose prediction differences between two versions of AAA and AXB algorithm led to the investigation of the key changes made from version 10.0.28 to version 13.6.23. For AAAv13.6, it was found that a layer of water with a thickness of half CT slice spacing was no longer automatically added to the surface of the medium contour.[37–39] Subsequently, AAAv13.6 dose calculation was also corrected from producing "staircases" in the dose distribution for the buildup region, especially when very low densities were present in that region.[38] AAA calculates doses based on the CT image electron density using a water-based dose kernel. It does not consider the material's elemental compositions. The layer of water added to the surface of the medium contour by AAAv10.0 previously was to approximate the surface and buildup doses within a water medium. This may be a good approximation for a static chest wall as shown in Fig. 8. However, for low HU value surfaces such as the moving chest wall, this approximation results in an overestimation of doses by AAAv10.0. Changes made in AAAv13.6 has shown that surface and buildup doses have better agreement with AXBv13.6 and MC calculations (Fig. 9).

For AXB algorithm, it was found that air medium was newly included in the material library of AXBv13.6.[22] Furthermore, AXBv13.6 currently allows the overlapping of mass density ranges in CT to material mapping.[22,21] Previously, AXBv10.0 assigns voxels with low HU values as low-density lung, in contrast to the air medium assigned by AXBv13.6. The difference in material assignment will result in different surface and buildup dose predictions due to different mass collision stopping powers and mass energy-absorption coefficients calculations. The overestimation of doses by AXBv10.0 in low HU value medium was also consistent with previous results from Ojala et al. and Onizuka et al. They compared the dose calculations of AXB version 10 against AXB version 11 within air medium.[23,24]

Other key changes for AAA and AXB algorithm version 13.6.23 include the improvement of image alignment and structure contouring in each voxel to calculation grid[37] and the changes made to the optimisation routine for the electron contamination model. The electron contamination model is sensitive to changes to dose deposition calculations and algorithm configuration routines.[40] The overall changes made to AAA and AXB algorithm in version 13.6.23 resulted in the agreement of dose prediction with MC benchmark as shown by the results in this study.

In addition, for small fields such as $2 \times 2\,cm^2$, AAA generally shows less agreement with AXB algorithm and MC simulations. Under small field conditions, there is an increase of lateral electronic disequilibrium along the central axis. AAA accounts tissue heterogeneity using the concept of radiological rectilinear scaling, where it simulates energy deposition as a function proportional to the ratio of the electron density of medium to water.[21] Rectilinear kernel scaling does not model small fields disequilibrium well as the different elemental composition of the simulated materials were disregarded. In reality, photon and electron scatter do not adhere to the rectilinear paths assumed in AAA. This is particularly pronounced in low-density lung material, where electron disequilibrium along the central axis becomes larger with smaller field sizes.[41] Furthermore, the previous study done by Fogliata et al. pointed out that AAA has an inability to model thin inhomogeneities accurately.[5] Changes in the HU value gradient (Fig. 2) were considered as several thin layers of heterogeneity as AAA assigns different electron densities to the voxel with respect to the voxel's HU value. These discrepancies were most noticeable in dose regions when there was a presence of a high HU value gradient as predicted by AAAv10.0 in Fig. 9. This results in the discrepancies between AAA, MC and AXB algorithm.

The limitation of this study was not validating the considered depth doses by conducting dosimetric measurements. Although dosimetric measurements will prove to be a robust standard, in-vivo dosimetric measurements will introduce several other challenges. The low density of the lung insert, as well as small field sizes such as $2 \times 2\,cm^2$, causes potential loss of charged particle equilibrium. This will result in significant perturbation to the energy spectrum and the detector's dose response. Perturbation corrections must therefore be applied to correct the change in dose response. These corrections can only be accurately pre-calculated using MC simulation of the detector in the measured medium. Eventually, the accuracy of the detector's dose reading will still be dependent on the accuracy of the MC simulation. Furthermore, the position of measurement will be challenging to justify due to the 1 cm amplitude sinusoidal motion. For instance, the surface dose measurement of the moving chest wall at depth 0 cm will be difficult to obtain as the detector will most likely to measure doses at the equilibrium of the sinusoidal motion at depth 1 cm, resulting in greater dosimetric discrepancies.

6. Conclusions

AAAv13.6 and AXBv13.6 proved to be more competent in extreme inhomogeneous dose prediction than AAAv10.0 and AXBv10.0. Key changes between version 10.0.28 and version 13.6.23 were identified for both AAA and AXB algorithm. With different dose prediction response, physicists and clinicians should consider the version of clinical algorithm used for dose calculation of treatment plans with extreme inhomogeneities and motion artefacts.

Conflict of interest

None declared.

Financial disclosure

None declared.

Acknowledgements

This work was supported by the Singapore National Research Foundation, Prime Minister's Office, under a Competitive Research Programme (Non-volatile Magnetic Logic and Memory Integrated Circuit Devices, NRF-CRP9-2011-01), and an Industry-IHL Partnership Program (NRF2015-IIP001-001). The work was also supported by a MOE-AcRF Tier 2 Grant (MOE

2013-T2-2-017). W.S. Lew is a member of the Singapore Spintronics Consortium (SG-SPIN).

REFERENCES

1. Huang L, Park K, Boike T, et al. A study on the dosimetric accuracy of treatment planning for stereotactic body radiation therapy of lung cancer using average and maximum intensity projection images. *Radiother Oncol* 2010;**96**(1):48–54.
2. Fogliata A, Nicolini G, Vanetti E, Clivio A, Cozzi L. Dosimetric validation of the anisotropic analytical algorithm for photon dose calculation: fundamental characterization in water. *Phys Med Biol* 2006;**51**:1421–38.
3. Van Esch A, Tillikainen L, Pyykkonen J, et al. Testing of the analytical anisotropic algorithm for photon dose calculation. *Med Phys* 2006;**33**(11):4130–48.
4. da Rosa LA, Cardoso S, Campos L, Alves VG, Batista D, Facure A. Percentage depth dose evaluation in heterogeneous media using thermoluminescent dosimetry. *J Appl Clin Med Phys* 2010;**11**:1.
5. Fogliata A, Nicolini G, Clivio A, Vanetti E, Cozzi L. Dosimetric evaluation of Acuros XB Advanced Dose Calculation algorithm in heterogeneous media. *Radiat Oncol* 2011;**6**:82.
6. Rana S, Rogers K, Pokharel S, Lee T, Reed D, Biggs C. Acuros XB algorithm vs. anisotropic analytical algorithm: a dosimetric study using heterogeneous phantom and computed tomography (CT) data sets of esophageal cancer patients. *J Cancer Ther* 2014;**4**:138–44.
7. Fogliata A, Nicolini G, Clivio A, Vanetti E, Cozzi L. Accuracy of Acuros XB and AAA dose calculation for small fields with reference to RapidArcVR stereotactic treatments. *Med Phys* 2011;**38**(11):6228–37.
8. Ojala J, Kapanen M, Sipilä P, Hyödynmaa S, Pitkänen M. The accuracy of Acuros XB algorithm for radiation beams traversing a metallic hip implant – comparison with measurements and Monte Carlo calculations. *J Appl Clin Med Phys* 2014;**15**:5.
9. Fogliata A, Cozzi L. Dose calculation algorithm accuracy for small fields in non-homogeneous media: the lung SBRT case. *Phys Med* 2016;**44**:157–62.
10. Dunn L, Lehmann J, Lye J, et al. National dosimetric audit network finds discrepancies in AAA lung inhomogeneity corrections. *Phys Med* 2015;**31**(5).
11. Ong C, Verbakel WF, Cuijpers JP, Slotman BJ, Senan S. Dosimetric impact of interplay effect on rapidarc lung stereotactic treatment delivery. *Int J Radiat Oncol Biol Phys* 2011;**79**(1):305–11.
12. Olding T, Garcia L, Alexander K, Schreiner LJ, Joshi C. Stereotactic body radiation therapy delivery validation. *J Phys Conf Ser* 2013;**444**(1):012073.
13. Kawrakow I, Mainegra-Hing E, Rogers DWO, Tessier F, Walters BRB, Tech. Rep. PIRS-701 *The EGSnrc code system: Monte Carlo simulation of electron and photon transport*. National Research Council Canada; 2015. URL: http://nrc-cnrc.github.io/EGSnrc/doc/pirs701-egsnrc.pdf.
14. Capote R, Jeraj R, Ma CM, et al, Tech. Rep. INDC(NDS)-0484 *Phase-space database for external beam radiotherapy Summary report of a consultants' meeting*. International Atomic Energy Agency (IAEA); 2006.
15. Rogers DWO, Walters BRB, Kawrakow I, Tech. Rep. PIRS-509(A)revL *The BEAMnrc users manual*. National Research Council Canada; 2016. URL: http://nrc-cnrc.github.io/EGSnrc/doc/pirs509a-beamnrc.pdf.
16. Hasenbalg F, Fix MK, Born EJ, Mini R, Kawrakow I. VMC++ versus BEAMnrc: a comparison of simulated linear accelerator heads for photon beams. *Med Phys* 2008;**35**:1521–31.
17. Zvolanek K, Ma R, Zhou C, et al. Still equivalent for dose calculation in the Monte Carlo era? A comparison of free breathing and average intensity projection CT datasets for lung SBRT using three generations of dose calculation algorithms. *Med Phys* 2017;**44**:1939–47, http://dx.doi.org/10.1002/mp.12193.
18. Han T, Mikell JK, Salehpour M, Mourtada F. Dosimetric comparison of Acuros XB deterministic radiation transport method with Monte Carlo and model-based convolution methods in heterogeneous media. *Med Phys* 2011;**38**(5):2651–64.
19. Bush K, Gagne IM, Zavgorodni S, Ansbacher W, Beckham W. Dosimetric validation of Acuros® XB with Monte Carlo methods for photon dose calculations. *Med Phys* 2011;**38**(4):2208–21.
20. Kan MWK, Leung LHT, Yu PKN. Verification and dosimetric impact of Acuros XB algorithm on intensity modulated stereotactic radiotherapy for locally persistent nasopharyngeal carcinoma. *Med Phys* 2012;**39**(8):4705–14.
21. Varian Medical Systems, Report P/N B502679R01B *Eclipse Algorithms Reference Guide*. Palo Alto, CA: Varian Medical Systems, Inc.; 2010.
22. Varian Medical Systems, Report P1008611-003-C *Eclipse Algorithms Reference Guide*. Palo Alto, CA: Varian Medical Systems, Inc.; 2015.
23. Onizuka R, Araki F, Ohno T, et al. Accuracy of dose calculation algorithms for virtual heterogeneous phantoms and intensity-modulated radiation therapy in the head and neck. *Radiol Phys Technol* 2016;**9**(1):77–87.
24. Ojala J, Kapanen M. Quantification of dose differences between two versions of Acuros XB algorithm compared to Monte Carlo simulations – the effect on clinical patient treatment planning. *J Appl Clin Med Phys* 2015;**16**(6).
25. Han D, Bayouth J, Bhatia S, Sonka M, Wu X. Characterization and identification of spatial artifacts during 4D-CT imaging. *Med Phys* 2011;**38**(4):2074–87.
26. Low DA, Harms WB, Mutic S, Purdy JA. A technique for the quantitative evaluation of dose distributions. *Med Phys* 1998;**25**(5):656–61.
27. van Battum LJ, Hoffmans D, Piersma H, Heukelom S. Accurate dosimetry with GafChromic EBT film of a 6 MV photon beam in water: what level is achievable? *Med Phys* 2008;**35**(2):704–16.
28. Ramaseshan R, Kohli K, Cao F, Heaton R. Dosimetric evaluation of plastic water diagnostic therapy. *J Appl Clin Med Phys* 2008;**9**(2):98–111.
29. Chang KP, Hung SH, Chie YH, Shiau AC, Huang RJ. A comparison of physical and dosimetric properties of lung substitute materials. *Med Phys* 2012;**39**(4):2013–20.
30. Fried R, Grimaldi J. *The psychology and physiology of breathing: in behavioral medicine, clinical psychology, and psychiatry*. Springer Science and Business Media; 1993. p. 165 [Chapter 5].
31. Zhang R, Feygelman V, Harris E, Rao N, Moros E, Zhang G. Is wax equivalent to tissue in electron conformal therapy planning? A Monte Carlo study of material approximation introduced dose difference. *J Appl Clin Med Phys* 2013;**14**:1.
32. Metrodent. *Metrodent Waxes Safety Data Sheet*; 1998. Available from: http://metrodent.com/pdfs/data-sheets.
33. *Chemical Abstracts Service Substance Details CAS Registry Number: 9002-81-7*; 2017. URL: http://www.commonchemistry.org/ChemicalDetail.aspx?ref=9002-81-7.
34. Olson JR, Liu CJ, Tian Y, Shen Q. Theoretical wood densitometry II. Optimal X-ray energy for wood density measurement. *Wood Fiber Sci* 1988;**20**:187–96.
35. Sun Y, Ge H, Cheng S, et al. Evaluation of interfractional variation of the centroid position and volume of internal target volume during stereotactic body radiotherapy of lung

cancer using cone-beam computed tomography. *J Appl Clin Med Phys* 2016;**17**(2):461–72.
36. Sixel KE, Ruschin M, Tirona R, Cheung PCF. Digital fluoroscopy to quantify lung tumor motion: potential for patient-specific planning target volumes. *Int J Radiat Oncol Biol Phys* 2003;**57**(3):717–23.
37. Varian Medical Systems, Report P1003988-010-J *Eclipse Distributed Calculation Framework, 13.0 MR3*. Palo Alto, CA: Varian Medical Systems, Inc.; 2016.
38. Varian Medical Systems, Report P1003988-010-J *Eclipse Distributed Calculation Framework, Version 13.5.35*. Palo Alto, CA: Varian Medical Systems, Inc.; 2016.
39. Varian Medical Systems, Report P1011139-005-E *Eclipse Distributed Calculation Framework, Version 13.6 MR 0.5*. Palo Alto, CA: Varian Medical Systems, Inc.; 2016.
40. Varian Medical Systems, Report B504900R01E *Eclipse Distributed Calculation Framework, Version 11.0, Build 11.0.32*. Palo Alto, CA: Varian Medical Systems, Inc.; 2016.
41. Tillikainen L, Helminen H, Torsti T, et al. A 3D pencil-beam-based superposition algorithm for photon dose calculation in heterogeneous media. *Phys Med Biol* 2008;**53**(14):3821.